Available online at www.sciencedirect.com
SciVerse ScienceDirect
Ceramics International 39 (2013) 6577–6581
CERAMICS INTERNATIONAL
www.elsevier.com/locate/ceramint

Effects of thermal annealing on the optical properties of Ar ion irradiated ZnS films

Shuwen Xue

Department of Physics, Zhanjiang Normal College, Zhanjiang 524048, China

Received 20 December 2012; received in revised form 25 January 2013; accepted 25 January 2013
Available online 8 February 2013

Abstract

Ar-ion-implantation to a dose of 1×10^{17} ions/cm^2 was performed on cubic ZnS thin films with (111) preferred orientation deposited on fused silica glass substrates by vacuum evaporation. After ion implantation, ZnS films were annealed in flowing argon at different temperatures from 400 to 800 °C. The effects of ion implantation and post-thermal annealing on the structural and optical properties of ZnS films were investigated by X-ray diffraction (XRD), photoluminescence (PL) and optical transmittance measurements. XRD reveals that the diffraction peaks recover at ~500 °C. The optical transmittances show that the bandgap of ZnS films blueshifts when annealed below 500 °C, and redshifts when annealed above 500 °C. PL results show that the intrinsic defect related emissions decrease with increasing annealing temperature from 400 to 500 °C, and increase with increasing annealing temperature from 500 to 800 °C. The observed PL emissions at 414 and 439 nm are attributed to the transitions of $Zn_i \rightarrow V_{Zn}$ and $V_S \rightarrow$ VBM, respectively.
© 2013 Elsevier Ltd and Techna Group S.r.l. All rights reserved.

Keywords: ZnS; Ion implantation; PL; XRD

1. Introduction

Zinc sulfide (ZnS), an important II–VI semiconductor with a variety of good physical and chemical properties, is suitable for many applications like thin film solar cells, light emitting diodes and electroluminescent devices [1–3]. Up to now, many techniques have been developed to synthesize high-quality ZnS films, such as radio frequency (RF) magnetron sputtering, molecular beam epitaxy, pulsed laser deposition, chemical vapor deposition, chemical bath deposition and vacuum evaporation [4–8]. Among them, the vacuum evaporation technique is the more convenient way to prepare ZnS thin films.

For special applications, ZnS must be doped with proper impurity elements. Ion implantation, especially in the semiconductor industry, is a widespread tool for doping semiconductors. It has been used to fabricate n- and p-type ZnS [9,10]. The advantages of ion implantation are the lateral selectivity of the sample area and doping depth as well as an accurate dose control. In principle, every element from the periodic system can be implanted, which makes it a multipurpose and flexible tool for doping semiconductors. However, undesirable side effects are the implantation-induced damage and its effects on the structural, optical and electrical properties of the semiconductor. To eliminate the undesirable side effects induced by ion implantation, thermal annealing and laser annealing are usually adopted. Though some efforts have been made to dope ZnS for special purposes by ion implantation, ion-beam-induced damage and its effects and elimination by thermal annealing are not clear. In addition, as a well-known phosphor, the photoluminescence of ZnS has received wide attention in recent years. However, the mechanism of the photoluminescence of ZnS is still under debate, especially for the defect-related blue emissions in the visible region [11–13].

In this work, ZnS films were prepared with a conventional vacuum evaporation method. In order to investigate the ion-beam-induced damage and its effects and elimination by thermal annealing, we perform Ar-ion-implantation on the ZnS films to avoid the effects induced by the incorporation of implanted element in ZnS lattice. The Ar-implanted ZnS films were annealed in flowing argon at different temperatures from 400 to 800 °C. The effects of ion implantation and post-thermal annealing on the structural and optical properties were studied.

E-mail address: xueshuwen@263.net

0272-8842/$ - see front matter © 2013 Elsevier Ltd and Techna Group S.r.l. All rights reserved.
http://dx.doi.org/10.1016/j.ceramint.2013.01.092

2. Experimental

ZnS thin films were deposited on fused silica glass substrates by the vacuum evaporation method. Before deposition, the substrates were first ultrasonically cleaned in acetone for 10 min to remove the organic contamination on the surface, and then washed in deionized water for 5 min. Subsequently, the substrates were again ultrasonically cleaned in alcohol for 10 min to further remove the surface contamination and were washed by deionized water for 5 min. Then the substrates were rinsed in HF (5 at%) solution for 5 min to remove the surface oxide. Finally, the substrates were washed in deionized water for 5 min and dried in thermal floating air. The substrates were then transferred into the vacuum chamber, which was pumped to about 1×10^{-4} Pa with a combination of mechanical pump and diffusion pump. To further remove the absorbed gas and residual contamination on the substrate surface, the substrates were heated for 10 min, and then high-purity ZnS powders on a tungsten crucible were heated by Joule's effect. ZnS films were deposited at a substrate temperature of 200 °C.

The as-prepared films were subjected to Ar ion implantation at 56 keV to a dose of 1×10^{17} ions/cm^2. After ion implantation, Ar-implanted films were annealed in flowing argon at different temperatures from 400 to 800 °C for 1 h in a quartz tube furnace.

To characterize the structural and optical properties of ZnS films, the surface morphology was scanned using a SPA-300HA atomic force microscope (AFM), the crystal orientation was investigated using a PHILIPS X'PERT PRO MPD X-ray diffractometer (XRD) with the radiation source of CuKα, the optical transmittance was measured using a SHIMADZU UV2550 spectrophotometer, the room temperature (RT) photoluminescence spectra (PL) were recorded by a SHIMADZU RF5301PC spectrophotometer with excitation wavelength of 360 nm.

3. Results and discussion

3.1. Characterization of as-prepared ZnS films

Fig. 1(a) shows the typical AFM images of the as-prepared ZnS films deposited on fused silica glass substrates by the vacuum evaporation process. The minimum root-mean square of the surface roughness is about 1.55 nm. The average grain size is ~59 nm. The surface of the as-prepared ZnS films is very smooth. X-ray diffraction patterns of the as-prepared ZnS films are shown in Fig. 1(b). Only the diffraction peak at $2\theta\approx28.6^\circ$ appears in the pattern. It is well known that ZnS has two commonly available allotropes: one with a zinc blende (ZB) structure and the other with a hexagonal wurtzite (WZ) structure. Whereas the (111) peak of ZB ZnS and the (002) peak of WZ ZnS are very close, the cubic form is the stable low-temperature phase, while the latter is the high-temperature polymorph which forms at around 1296 K [14]. Therefore, the diffraction peak can be indexed to the cubic ZnS. It can also be seen that no other phase appears in the XRD patterns. It shows that the as-prepared ZnS films exhibit the ZB structure with (111) preferred orientation.

3.2. Influences of ion implantation and post-thermal annealing

3.2.1. Structural properties

To investigate the effects of thermal annealing on the structural properties of Ar-implanted ZnS films, the films were annealed in flowing argon at different temperatures from 400 to 800 °C for 1 h after ion implantation. Fig. 2 shows the XRD patterns of ZnS films after ion implantation and annealing at different temperatures. It can be seen that the diffraction peak of (111) disappears from the XRD patterns after Ar ion implantation. This implies that the lattice of ZnS films is heavily destroyed after high-dose ion-implantation. The disappearance of the diffraction peak can be attributed to the ion-beam induced lattice disorder. The Ar-implanted ZnS films were subsequently subjected to thermal annealing to repair the ion-beam induced lattice disorder. It can be seen from Fig. 2 that thermal annealing has great influences on the structural recovery of Ar-implanted ZnS films. The results show that the diffraction peak of (111) appears again after the ZnS films annealed at 400 °C for 1 h, and the ZnS films still remain ZB structure. But the intensity of (111) diffraction peak is very weak. This suggests that the lattice of Ar-implanted ZnS films is partially repaired. Further annealing at 500 °C for 1 h sees a full structural recovery of Ar-implanted ZnS films. With increasing the annealing temperature from 500 to 700 °C, we can see that the (111) diffraction peak is intensified, and the full width at the half maximum (FWHM) of (111) decreases gradually. This implies that the crystallinity of the ZnS films improves and the grain size increases. However, the intensity of (111) peak decreases with increasing the annealing temperature beyond 700 °C. This may be due to the thermally induced lattice disorder at high temperature. It is noted that the lattice recovery of the Ar-implanted ZnS films occurs after annealing at 500 °C for 1 h.

3.2.2. Optical properties

Fig. 3 shows the influences of Ar ion implantation and thermal annealing on the optical transmittance of ZnS films. It can be seen from Fig. 3 that the optical transmittance was decreased distinctly in the visible region after Ar ion implantation. It is known that ion implantation can introduce a great deal of point defects (such as vacancies, interstitials and antisites) or defect complex in the host materials due to the strong collisions between the incident ion and host lattice. These defects usually enhance the optical absorption in the host materials. Subsequent annealing has evident influences on the optical transmittance of Ar-implanted ZnS films. It is found that the optical transmittance in the visible region increases when increasing the annealing temperature from

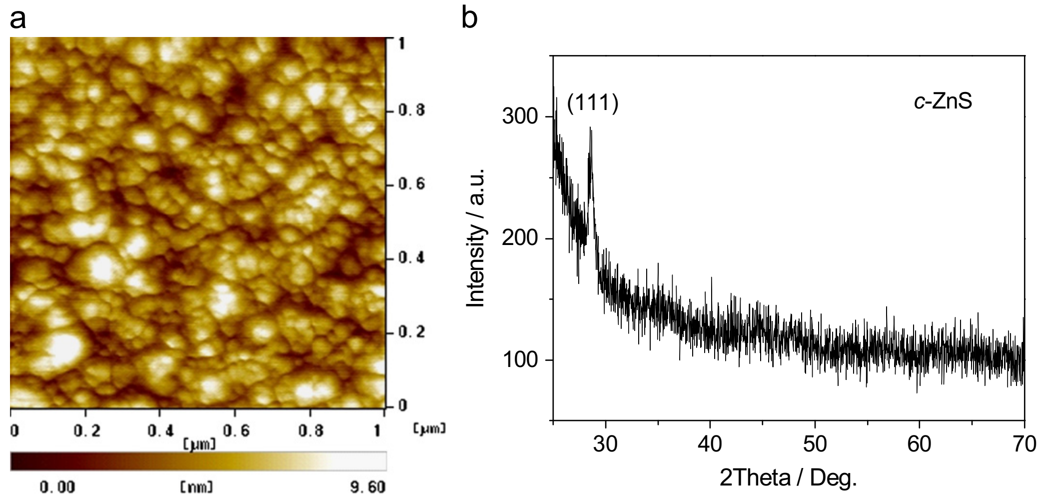

Fig. 1. (a) Typical AFM image and (b) XRD pattern of as-prepared ZnS film.

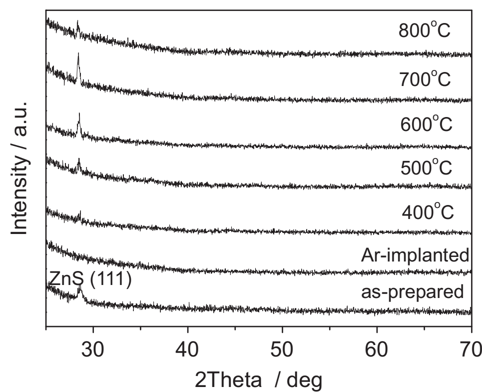

Fig. 2. XRD patterns of ZnS films after ion implantation and post-thermal annealing at different temperatures.

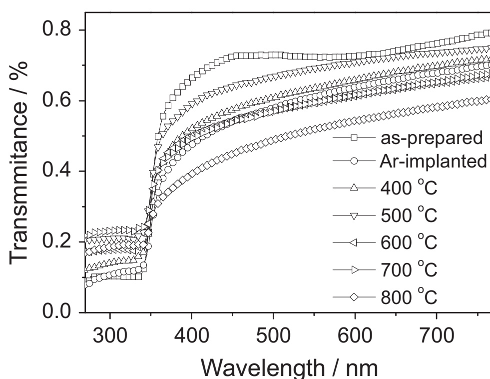

Fig. 3. Optical transmittance spectra of ZnS films after ion implantation and post-thermal annealing at different temperatures.

400 to 500 °C. However, it decreases dramatically when increasing the annealing temperature above 500 °C. We think that the observed behaviors of optical transmittance may be mainly due to the changes of defect concentrations in ZnS films after ion implantation and thermal annealing. As discussed in the structural analysis, a great deal of defects can be produced during ion implantation and high-temperature annealing. These defects serve as trapped electron centers and can effectively affect optical absorption [15,16]. The ion-beam-induced defects can be gradually annealed out by annealing at 400–500 °C, which results in the enhancement of optical transmittance in the visible region, i.e. the recovery of optical transmittance of ZnS films. However, thermally induced defects increase dramatically during the following annealing stage between 500 and 800 °C. This results in the increase of the optical absorption again. It is noted that the optical absorption in the visible region nearly recovers after annealing at 500 °C, indicating that most of the ion-beam-induced defects are annealed out. This is essentially in agreement with XRD analysis.

In addition, Ar ion implantation and post-thermal annealing also have distinct influences on the optical bandgaps of ZnS films as shown in Fig. 4. The optical bandgaps are determined from the conventional method [17]. It can be seen from the inset of Fig. 4 that the optical bandgap redshifts after Ar ion implantation. Subsequent annealing between 400 and 500 °C makes the optical bandgap blueshift, while redshift occurs between 500 and 800 °C. We also attribute the observed behaviors of the optical bandgaps mainly to the changes of defect concentrations in ZnS films. As mentioned above, many defects are produced during Ar ion implantation. The ion-beam-induced defects can form a great deal of defect states near the band edge. They cause the redshift of the optical bandgap. Because most of the ion-beam induced defects are annealed out by the subsequent annealing from 400 to 500 °C. We can see from Fig. 4 that the bandgap blueshifts due to the decrease of defect concentration in ZnS films. During the following annealing stage between 500 and 800 °C, thermally induced defects at high temperatures increase dramatically, which leads to the redshift of the optical band edge again due to the increase of defect concentration with annealing temperatures.

As mentioned above, ion implantation and high-temperature annealing cause structural disorders in ZnS films. This can also be reflected in the optical absorption band tail and can be characterized by empirical Urbach rule. The slope

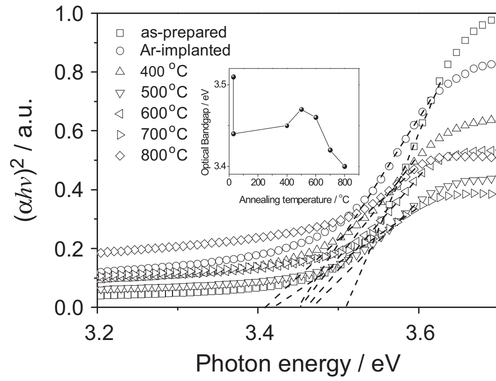

Fig. 4. Dependence of the optical bandgaps of ZnS films on ion implantation and post-thermal annealing.

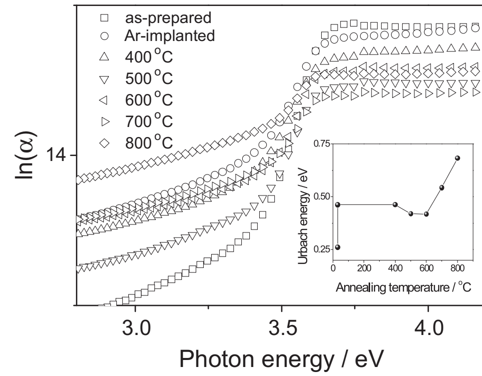

Fig. 5. Dependence of ln[α(λ)] on photon energy and Urbach energy as a function of annealing temperatures.

of the Urbach tail (Urbach energy) characterizes the structural disorder in the material and can be used to evaluate the defect concentrations in ZnS films. It is known that absorption coefficient $\alpha(\lambda)$ near the band edge shows an exponential dependence on photon energy [18]:

$$\alpha(\lambda)=\alpha_0\exp\left(\frac{h\upsilon}{E_0}\right), \quad (1)$$

where E_0 is the Urbach energy, α_0 is a constant. Thus, a plot of ln[α(λ)] versus photon energy should be linear and Urbach energy can be obtained from the slope. α(λ) can be obtained from the transmittance spectra of Fig. 3 using a simple model: $T=\exp[-\alpha(\lambda)d]$, where T is the optical transmittance and d is the thickness of ZnS films. In this work, the thickness of ZnS films is ~800 nm measured by a OLYMPUS BX51 interference/transmission microscopy. The dependence of ln[α(λ)] on wavelength is given in Fig. 5. Urbach energy can be calculated from the reciprocal gradient of the linear portion of the curves in Fig. 5 and is shown in the inset of Fig. 5. It can be seen that Urbach energy increases after Ar ion implantation and decreases when increasing the annealing temperature from 400 to 500 °C. This indicates that many defects are produced during Ar ion implantation and are gradually annealed out by the subsequent annealing at 400–500 °C. Further annealing at 500–800 °C makes Urbach energy increase again, indicating that thermally induced defects increase when increasing the annealing temperature. Urbach energy dependence on annealing temperature agrees well with the analysis above.

Fig. 6 shows RT PL spectra of ZnS films after ion implantation and annealing at different temperatures from 400 to 800 °C. It can be seen that all ZnS PL spectra exhibit two broad emission peaks centered at about 414 and 439 nm. The inset of Fig. 6 plots the dependence of the peak intensities of 414 and 439 nm emissions on the annealing temperatures. In this work, the ZnS films are nominally undoped. Therefore, the observed two emissions must come from the transitions between the intrinsic defect levels or the transitions between the intrinsic defect levels and band edge. According to the first-principle total-energy calculations of the native defects in ZnS [19], we find that the transition radiations from Zn interstitial (Zn_i) to Zn vacancy (V_{Zn}) and S vacancy (V_S) to the

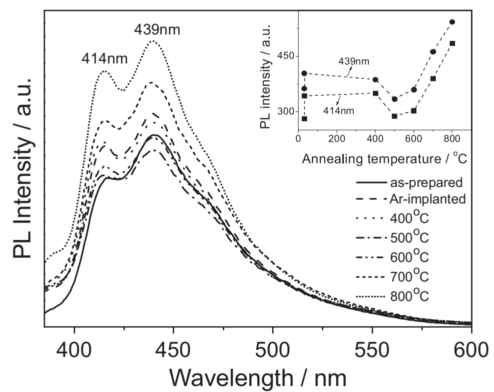

Fig. 6. RT PL spectra of ZnS films after ion implantation and post-thermal annealing at different temperatures.

valence band maximum (VBM) are very close to the 414 and 439 nm emissions, respectively. Therefore, we attribute the 414 nm emission to the transition of $Zn_i \rightarrow V_{Zn}$ and $V_S \rightarrow$ VBM as shown in Fig. 7. It is known that ion implantation can cause mainly point defects in the host materials. We can find from Fig. 6 that the 414 and 439 nm emissions enhance after Ar ion implantation. This implies that such intrinsic defects as Zn_i, V_{Zn} and V_S increase after Ar ion implantation. Subsequent thermal annealing at temperatures from 400 to 500 °C sees the decrease of the intensities of the 414 and 439 nm emissions due to the annealing out of the ion-beam-induced defects as mentioned above. However, the intensities of the 414 and 439 nm emissions enhance with further annealing at 500–800 °C. This can be attributed to the increases of thermally induced defects at higher temperatures. It is noted that the PL intensities nearly recover after annealing at 500 °C.

4. Conclusion

(111) preferred orientation cubic ZnS films deposited on fused silica glass substrates are subjected to Ar ion implantation. Ar ion implantation to a dose of 1×10^{17} ions/cm^2 has caused structural and optical changes to ZnS thin films. After Ar ion implantation, ZnS films still remain single phase and ZB structure. XRD intensities and PL

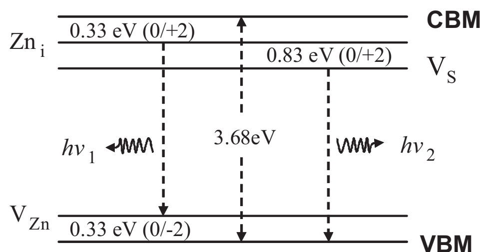

Fig. 7. The intrinsic defect levels in ZnS [19] and the possible transitions between the defect levels.

emissions are decreased by Ar ion implantation. Through post-implantation annealing, ion-implantation induced defects can be effectively annealed out. The structural and optical properties of Ar-implanted ZnS films nearly recover at ~500 °C. The observed PL emissions at 414 and 439 nm are attributed to the transitions of $Zn_i \rightarrow V_{Zn}$ and $V_S \rightarrow$ VBM.

References

[1] X.D. Gao, X.M. Li, W.D. Yu, Morphology and optical properties of amorphous ZnS films deposited by ultrasonic-assisted successive ionic layer adsorption and reaction method, Thin Solid Films 468 (2004) 43.

[2] S.H. Deulkar, C.H. Bhosale, M. Sharon, A comparative study of structural, compositional, thermal and optical properties of non stoichiometric (Zn,Fe)S chalcogenide pellets and thin films, Journal of Physics and Chemistry of Solids 65 (2004) 1879.

[3] J. Vidal, O. De Melo, O. Vigil, N. Lopez, G. Contreras-Puente, O. Zelaya-Angel, Influence of magnetic field and type of substrate on the growth of ZnS films by chemical bath, Thin Solid Films 419 (2002) 118.

[4] L.X. Shao, K.H. Chang, H.L. Hwang, Zinc sulfide thin films deposited by RF reactive sputtering for photovoltaic applications, Applied Surface Science 212 (2003) 305.

[5] I. Kunio, O. Toshikazu, K. Yoichi, F. Shizuo, F. Shigeo, Growth of ZnS and ZnCdSSe alloys on GaP using an elemental sulfur source by molecular beam epitaxy, Journal of Crystal Growth 138 (1994) 28.

[6] M. McLaughlin, H.F. Sakeek, P. Maguire, W.G. Graham, J. Molloy, T. Morrow, S. Laverty, J. Anderson, Properties of ZnS thin films prepared by 248nm pulsed laser deposition, Applied Physics Letters 63 (1993) 1865.

[7] A. Abounadi, M. Di Blasio, D. Bouchara, J. Calas, M. Averous, O. Briot, N. Briot, T. Cloitre, R.L. Aulombard, B. Gil, Reflectivity and photoluminescence measurements in ZnS epilayers grown by metal-organic chemical-vapor deposition, Physical Review B 50 (1994) 11677.

[8] S.H. Mohamed, M. El-Hagary, M. Emam-Ismail, Thickness and annealing effects on the optoelectronic properties of ZnS films, Journal of Physics D: Applied Physics 43 (2010) 075401.

[9] L.C. Olsen, R.C. Bohara, D.L. Barton, Vacuumevaporated conducting ZnS films, Applied Physics Letters 34 (1979) 528.

[10] Y. Tokuo, T. Shuhei, Li^+ ion implantation into ZnS epitaxial layers grown by metalorganic vapor phase epitaxy, Journal of Crystal Growth 117 (1992) 415.

[11] X.M. Meng, J. Liu, Y. Jiang, W.W. Chen, C.S. Lee, I. Bello, S.T. Lee, Structure- and size-controlled ultrafine ZnS nanowires, Chemical Physics Letters 382 (2003) 434.

[12] Q. Lai, L.I. Burtrand, K.M. Jong, J.E. Jae, C.Y. Jae, Synthesis and characterization of ZnS:Cu,Al phosphor prepared by a chemical solution method, Journal of Luminescence 104 (2003) 261.

[13] C. Ye, X. Fang, G. Li, L. Zhang, Origin of the green photoluminescence from zinc sulfide nanobelts, Applied Physics Letters 85 (2004) 3035.

[14] X.S. Fang, T.Y. Zhai, U.K. Gautam, L.A. Li, L.M. Wu, B. Yoshio, D. Golberg, ZnS nanostructures: from synthesis to applications, Progress in Materials Science 56 (2011) 175.

[15] J.H. Mackey, H.L. Smith, A. Halperin, Optical studies in x-irradiated high purity sodium silicate glasses, Journal of Physics and Chemistry of Solids 27 (1966) 1759.

[16] J.A. Cohen, G.G. Janezic, Relationships among trapped hole and trapped electron centers in oxidized soda–silica glasses of high purity, Physica Status Solidi A 77 (1983) 619.

[17] N. Kenny, C.R. Kannewurf, D.H. Whitmore, Optical absorption coefficients of vanadium pentoxide single crystals, Journal of Physics and Chemistry of Solids 27 (1966) 1237.

[18] F. Urbach, The long-wavelength edge of photographic sensitivity and of the electronic absorption of solids, Physical Review 92 (1953) 1324.

[19] Y.Q. Gai, J.B. Li, B. Yao, J.B. Xia, The bipolar doping of ZnS via native defects and external dopants, Journal of Applied Physics 105 (2009) 113704.